Thermal Imagery Spectral Analysis

Brian H. Collins[a], Richard C. Olsen[a], John Hackwell[b]

[a]Department of Physics, Naval Postgraduate School, Monterey, CA 93943-5002
[b]Aerospace Corporation, 2350 E. El Segundo Blvd, El Segundo, CA 90245-4691

ABSTRACT

Thermal imagery from the Spatially Enhanced Broadband Array Spectrograph System (SEBASS) was analyzed for target detection purposes. The push-broom sensor was operated as part of the WESTERN RAINBOW experiment in October 1995. Data from 7.8-13.4 microns were collected in 128 wavelength bands, with 128 pixels in the cross-track direction. The data set had a nominal ground-resolution of better than one meter. Analysis techniques normally used in the reflective domain, with traditional imaging spectrometers, were used for the thermal data. Analysis was done in both the radiance and emissivity domains, following careful thermal calibration and atmospheric compensation. The techniques utilized were principal components, spectral angle mapper, and spectral matched filter. All were successful, with the first two showing a success rate comparable to that found in similar experiments in the reflective domain. The principal components technique was successful in discriminating man-made objects and disturbed earth from the desert background, much as expected. It was also successful in distinguishing between different categories of man-made objects. Of the latter two techniques, the spectral matched filter was more successful. This relatively greater success is attributed to the sensitivity of the spectral angle mapper to calibration errors, particularly in the conversion from radiance to emissivity.

Keywords: hyperspectral, thermal, imagery, spectroscopy, LWIR, emissivity, WESTERN RAINBOW, target detection.

1. INTRODUCTION

Rapid advances in remote sensing technologies have led to new sensors which greatly improve our ability to gather information about distant objects without physical contact. While many of these sensors and technologies were designed for environmental monitoring and earth science, they may have important uses in the Department of Defense as today's warfighter strives to gain a complete picture of the battlespace around him. Hyperspectral imagery, one of the most promising of these emerging technologies, provides opportunities to discriminate between objects by detecting subtle differences in material spectral signatures. From the standpoint of military targeting and identification, this technology has the potential to defeat camouflage and concealment efforts and detect targets in a variety of background settings.

Most hyperspectral instruments, like the Airborne Visible/Infrared Imaging Spectrometer (AVIRIS)[1] and the Hyperspectral Digital Imagery Collection Experiment (HYDICE),[2] collect information in the region of the electromagnetic spectrum dominated by solar illumination. These instruments acquire a complete reflectance spectrum by recording the reflected solar radiation from an object. Although these sensors have achieved success in material identification, they are ineffective in the absence of solar illumination. Aerospace Corporation created SEBASS[3] to extend the range of hyperspectral sensors into the thermal infrared region. In contrast to the visible, the infrared region is dominated by thermal self-emission allowing the sensors to operate equally well during both day and night. By examining the emissivity differences between target objects in the same way that visible hyperspectral sensors examine differences in solar reflectivity, thermal infrared hyperspectral sensors have the potential to perform target detection, terrain categorization, and materials classification regardless of illumination conditions.

To study the utility of these sensors, long-wave infrared (LWIR) data were collected by SEBASS during Exercise WESTERN RAINBOW at the Yuma Proving Ground, AZ in October of 1995. The data were analyzed to determine the utility of an imaging thermal spectral sensor to support military operations. The study demonstrated the potential of this class of instrument to detect man-made objects, identify specific classes of materials, and perform terrain categorization.[4]

Airborne LWIR data were collected over a series of scenarios consisting of target vehicles arranged in a desert setting. This paper presents the results for a subset of the WESTERN RAINBOW data. The experiment setup, including a description of SEBASS and the collection scenarios, is presented in Section 2. Section 3 is a description of the data preparation procedures employed prior to analysis. The results of the analysis of the data using principal components analysis, a spectral matched filter, and the spectral angle mapper are presented in Section 4. Section 5 summarizes the conclusions drawn from the analysis of the SEBASS data.

2. EXPERIMENT DESCRIPTION

2.1 **SEBASS**

Thermal remote sensing development has followed a progression toward higher spectral resolution in the drive toward identifying materials based on their emissive spectra. The thermal infrared multispectral scanner (TIMS) demonstrated that contiguous, moderately narrow bands could be used to discriminate between various minerals based on their spectral features.[5] The analysis of data from Aerospace Corporation's non-imaging thermal spectral instrument, the Broadband Array Spectrograph System (BASS), demonstrated that hyperspectral LWIR measurements could detect fine spectral features and identify specific materials based on their spectral characteristics.[6] The success of BASS led to the development of SEBASS, an imaging infrared instrument based on BASS's dispersive, two-channel design.

SEBASS is a push-broom imaging device which consists of two spectrographs: one for the mid-wave infrared (MWIR) region (2.9-5.2 μm) and one for the LWIR region (7.8-13.4 μm).[3] Radiation entering SEBASS is split into the two spectrographs which focus a dispersed image of the slit onto 128 by 128 element impurity band conduction arrays. For the purpose of this study, only the LWIR channel was used. The spectral resolution of the LWIR channel varied from 0.063 μm on the short wavelength (7.8 μm) edge of the array to 0.035 μm at the long wavelength (13.4 μm) edge due to the characteristics of longwave radiation and the dispersion qualities of the channel's NaCl prism.

For data collection, SEBASS was mounted in a Twin Otter aircraft. The SEBASS cryostat was mounted on a platform that could be steered in the roll direction of the aircraft. A telescope with a focal length of one-meter focused the incoming radiation onto the instrument's field optics. The field-of-view of the telescope was one milliradian. From operating altitudes of 700 to 3000 ft, the ground sample distance (GSD) of SEBASS was 0.7 to 3.0 ft. A black and white camera and a MWIR camera were mounted on the Twin Otter to assist the operator in steering SEBASS and to aid in post-mission analysis of collected data.

2.2 **Collection scenarios**

In order to provide a realistic environment for target detection and classification, several collection sites were established. A mixture of military vehicles and decoys were emplaced at several sites according to tactical considerations and camouflage, concealment, and deception (CC&D) techniques.

The first collection site, the Malpai Site, consisted of a series of threat vehicles, camouflage schemes, decoys, and calibration panels. The target materials were placed on a background of desert pavement which consisted of small pebbles coated with a desert varnish. Vegetation was sparse and located in two washes that ran alongside the collection site. An array of five Soviet T-72 tanks was centered within the target site. The tanks were oriented in various directions to allow for multiple sun-angle geometries. In the north part of the site, a series of camouflage treatments and decoys were placed. These included US and Soviet color panels, prototype camouflage materials, and helicopter decoys. At the south end of the site, two US tanking vehicles were placed in the open.

The Arroyo Site was a simulation of a tactical ballistic missile (TBM) site. The site had a moderate amount of vegetation. The collection targets included two TBM positions, three defensive tanks, and an armored personnel carrier. The threat vehicles were arranged in a protective perimeter around the high value TBM targets. All of the targets within the Arroyo utilized some form of camouflage treatment.

2.3 **Additional collection equipment**

Several sensors were used to collect ground truth spectra from some of the target materials. These sensors included the Johns Hopkins University (JHU) micro Fourier transform imaging radiometer and the Environmental Institute of Michigan's (ERIM) Bomem MB-100 FTIR. In addition, JHU performed laboratory LWIR measurements of material samples with a Nicolet FTIR spectrometer and a Beckman grating spectrometer. The ground truth data were used to build a reference library for comparison with collected SEBASS data.

2.4 Sensor performance

WESTERN RAINBOW was the first operational use of SEBASS. Data were collected over the collection sites at an altitude of 2,500 ft producing images with a ground pixel size of 2.5 ft. The swath width of each data set was approximately 320 ft. Although the instrument performed extremely well throughout the exercise, three anomalies were noted in the collected data.

Intensely bright objects created a ghost image of themselves approximately ten lines ahead of their actual location. The problem was caused by the reflection and diffraction of incoming radiation as it interacted with the edge of the imaging slit. The ultimate effect was a mixing of scene radiance from each line with the line ten scans ahead of it.

The initial configuration of SEBASS exhibited a small degree of thermal drift. This drift was characterized through analysis of the calibration measurements taken throughout the experiment and accounted for during the conversion from instrument digital numbers to radiance values. The initial data from SEBASS also revealed that the gain of one of SEBASS's four amplifiers appeared to vary from flight to flight. Once the instrument was activated, the gain appeared constant. This variation was accounted for by comparing the output of the errant amplifier with its adjacent amplifiers. These problems have since been corrected in the instrument, but affect all of the data collected during the experiment.

3. HYPERSPECTRAL OBSERVATIONS

Data collected over each collection site were analyzed using several hyperspectral analysis techniques. Prior to analysis, the data were converted from raw instrument digital number into several data formats: radiance measured at the sensor (radiometrically calibrated data), a simulated FUR image, and apparent emissivity.

3.1 Spectral and radiometric calibration

The first step in data processing was spectral and radiometric calibration. The spectral calibration of SEBASS was accomplished by placing a polymer film over the aperture as the instrument imaged a blackbody at a known temperature. The location of known absorption features within the film were used to generate a polynomial function which described the wavelength for each pixel in the array.[7] The process for converting instrument digital number to actual radiance values, $W/cm^2 \mu m$ sr, was accomplished through the use of on-board blackbodies and a non-linear calibration technique devised by B. Johnson.[8]

3.2 Simulated single-band FLIR image

After the SEBASS data were spectrally and radiometrically calibrated, a simulated, single-band FLIR image was generated. This image was generated by averaging the radiance values measured in each band. It served as the standard image with which to compare the results of analysis of the spectral data.

3.3 Atmospheric correction

Atmospheric correction was a two-step process. Relative atmospheric transmittance and upwelling radiance for each data set were determined using a technique referred to as the plastic ruler technique. This technique was developed to derive atmospheric parameters for infrared hyperspectral collections using in-scene data.[9] The plastic ruler algorithm assumes that a large number of scene elements have emissivities close to 1.0 so that infrared radiation reaching the sensor from a source on the ground equals

$$L_{sensor} = \tau\, B(T) + L_{upwelling} \qquad (1)$$

where τ is the atmospheric transmittance, ***B (T)*** is the radiance emitted by a blackbody at temperature ***T,*** and $L_{upwelling}$ is the atmospheric upwelling radiance. For scenes that include a moderate amount of vegetation, which exhibits a near blackbody radiation curve in the LWIR region, equation (1) applies to a large number of data points within the scene. τ and $L_{upwelling}$ are calculated by determining the slope and offset of a scatter plot of measured vs. emitted radiance for a representative set of data points. Figure 1 is a sample scatter plot of data values in a single wavelength band. For each point, the surface temperature has been estimated by assuming that the maximum brightness temperature of the data point represents its temperature. The amount of radiation emitted by a blackbody at this estimated temperature is then plotted against the radiance measured by the sensor. The plastic ruler method solves for τ and $L_{upwelling}$ by drawing a line through the upper bound of the scatter plot which represents scene elements with emissivities close to 1.0.

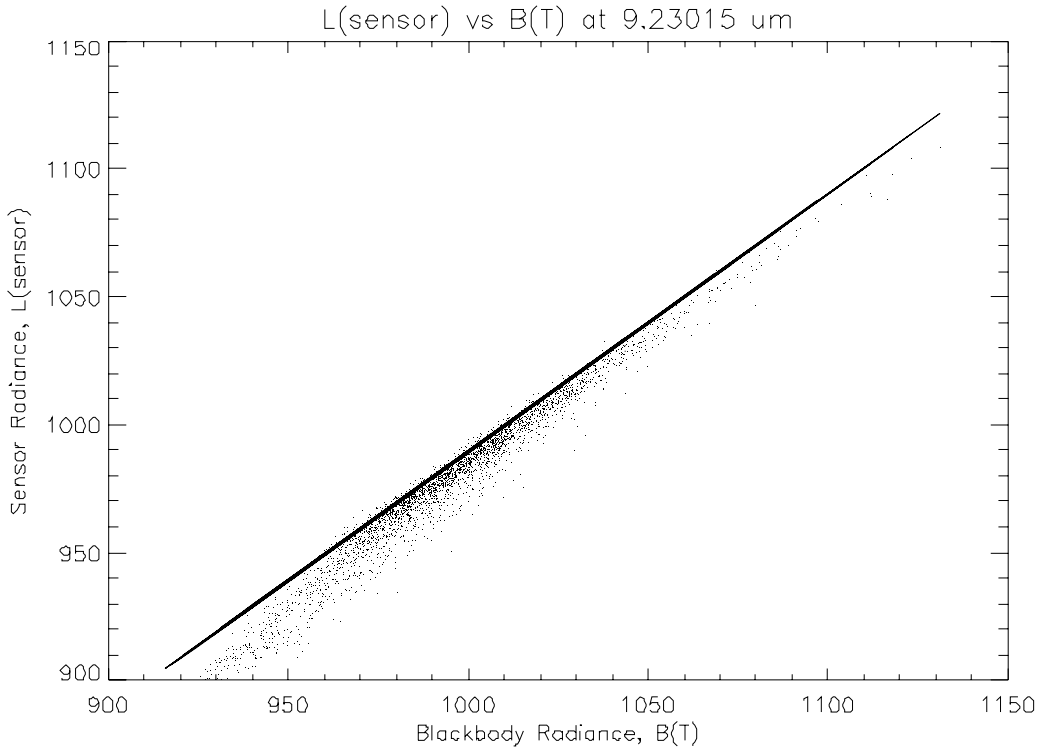

Figure 1. Scatter plot of measured radiance vs. blackbody radiance for a single band.

The data collected in this experiment consisted almost entirely of desert sand with little or no vegetation. As a result, the majority of the data points consisted of silicate-based minerals which exhibit strong spectral features within the LWIR region. The nature of Si-O bonds cause fundamental vibrational absorption resonances, called restrahlen bands, which appear as minima in emissivity spectra between 8.0 and 11.0 μm. Since the above procedure assumed that the scene included at least a moderate amount of near-blackbody materials (vegetation), application of the plastic ruler algorithm resulted in atmospheric transmittance and upwelling radiance values which were artificially weighted by the restrahlen feature of the sand. In order to lessen this effect, pixels which exhibited a strong restrahlen feature were excluded from the set used to derive the atmospheric parameters. Figure 2 depicts the results of the atmospheric correction procedure for data collected over the Malpai collection site.

The initial assumption that the emissivity of each scene element equals 1.0 somewhere within its spectrum results in relative atmospheric parameters instead of absolute corrections. The derivation of actual atmospheric parameters was accomplished by combining the plastic ruler method with Aerospace Corporation's ARTSPEC atmospheric modeling program. Using a procedure outlined by Burke,[10] the ARTSPEC model inputs were varied until the model's results exhibited the same relative shape as the plastic ruler results. These results were then used to scale the plastic ruler atmospheric correction factors.

The scaled atmospheric parameters were then applied to the SEBASS data by inverting equation (1) to remove the effects of the atmosphere and convert radiance measured at the sensor to radiance emitted by the source.

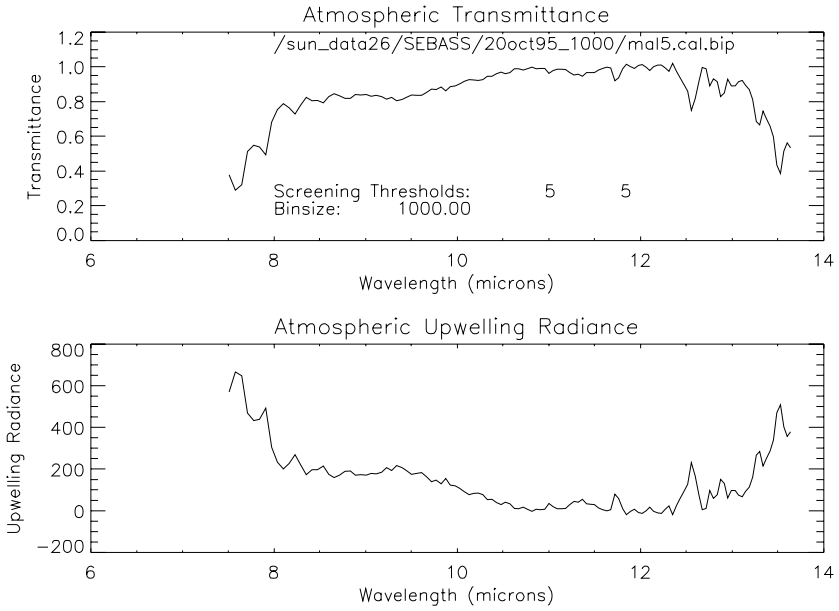

Figure 2. Results of Plastic Ruler atmospheric compensation technique (before scaling), Malpai Site.

3.4 Apparent emissivity

The conversion process from radiance emitted by the source to apparent emissivity began with the estimation of the surface temperature. For each pixel, brightness temperature was calculated by inverting the Planck function. The maximum brightness temperature measured within the bandwidth of the instrument was assumed to equal the surface temperature of the pixel. This estimation is based on the assumption that the emissivity maximum occurs somewhere between 8.0 and 13.0 1.m and is close to 1.0. Apparent emissivity was then calculated by computing the ratio of the radiation emitted by the source to the radiance emitted by a blackbody at the assumed surface temperature.

3.5 Hyperspectral analysis algorithms

A variety of analysis algorithms have been developed to analyze hyperspectral data. These range from algorithms which find matches for particular target spectra to those which detect anomalous spectra within a scene.[11] Three representative algorithms were applied to the SEBASS data: principle components analysis (PCA),[12] the spectral angle mapper (SAM),[13],[14] and a spectral matched filter (SMF).[15],[16]

4. DATA ANALYSIS

The SEBASS data collected in the experiment were analyzed to determine whether thermal spectral data can be used to detect targets in a military scenario. The analysis began with an intensive study of the Malpai Site. This data was used to establish a standard method of applying the hyperspectral analysis algorithms and served as a source of additional reference spectra to augment the ground truth spectra collected at the scene.

4.1 Malpai collection site

The Malpai data selected for analysis were collected at 10:00 local time on 29 October. The data were prepared using the procedures outlined in Section 3. Initial analysis began with an examination of the simulated FUR image (Figure 3) to determine how well various materials could be differentiated by thermal contrast. Almost all of the targets within the Malpai collection site were easily distinguishable from the desert varnish because of the high temperature of the desert surface. Some man-made materials, such as the calibration panels and several elements within the JCCD array, differed in temperature from the other man-made objects due to thermal inertia or emissivity differences and were also easy to

distinguish. On the other hand, the vegetation and tanks appeared similar and would be difficult to differentiate in a lower resolution image.

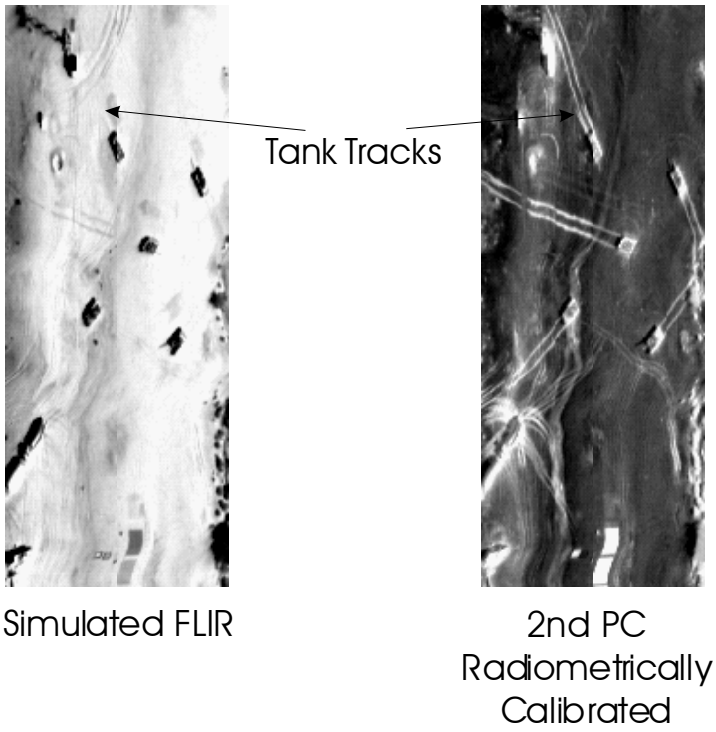

Figure 3. Simulated FLIR image and second PC image of radiometrically calibrated data, Malpai Site.

Principal components analysis of the Malpai data demonstrated that the target materials could be differentiated from each other as well as the background vegetation and sand. In addition, disturbances within the background sand, such as that caused by vehicular traffic, could also be detected. The principal components transform was applied to the radiometrically calibrated SEBASS data. Over 90% of the original scene variance was contained in the first principal component (PC), which is typically a weighted average of all of the bands of an instrument. In this case, the first PC produced an image similar to the simulated FLIR image and exploited the temperature variations within the scene allowing materials to be detected based on their surface temperature, thermal inertia properties, or internal heat. Each successive PC contained less and less of the information contained in the original data. The second PC provided a large amount of information about the scene which was not present in the simulated FLIR image or the first PC image. Figure 3 depicts the second PC image of the five-tank array alongside the simulated FLIR image. The weighting factors for this component highlighted materials which differed from the desert varnish background. As a result, materials with a high emissivity in the 8.0 to 9.0 μm restrahlen region appear bright. Tank tracks, desert surface variations, and the T-72 array were all clearly visible. The third PC displayed some additional discrimination capabilities and allowed targets to be discriminated from the background more clearly. Although the second and third PC images were useful in discriminating between man-made objects and the desert background, they did not provide much information to differentiate between types of man-made materials. Several of the higher components provided this capability allowing the calibration panels, foxhole cover, and bomb crater decoy to be easily distinguishable from both the background and the T-72 tanks.

Figure 4 displays how each spectral band was weighted to generate the first, second, and eighth PCs. As expected, the first PC is essentially a weighted average of the spectral bands. The second PC emphasizes spectral measurements within the restrahlen band of the desert sand. Since the eighth PC differentiated between elements within the JCCD array, the weighting function appeared to exploit specific spectral differences between these materials. Figure 8 (color page) is a composite image formed by combining these three PCs into a single red-green-blue image. The use of PC number eight

aided in the discrimination between the decoy materials, the calibration panels, and the T-72 tanks. In the composite image, the desert varnish is magenta and the background vegetation is yellow. The various man-made objects vary in color from orange in the case of the T-72 tanks to green and blue in the case of the JCCD decoy materials.

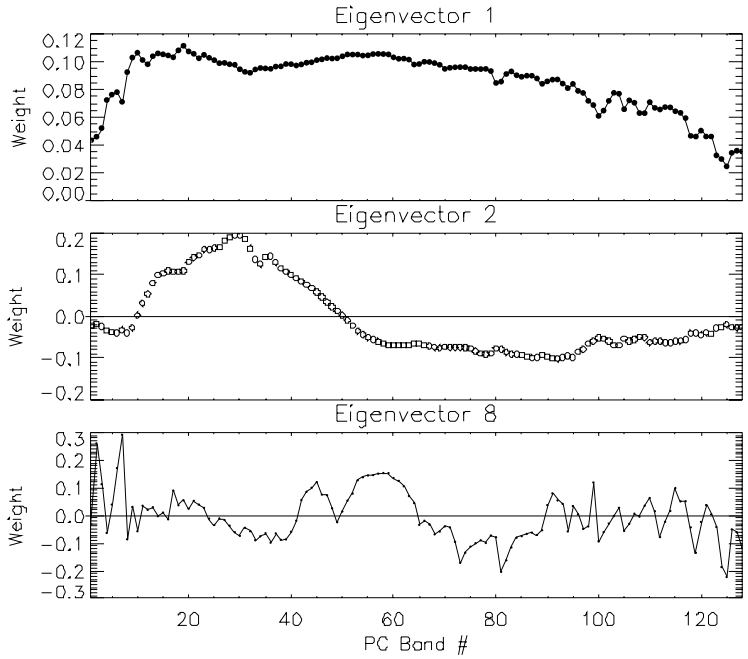

Figure 4. Weighting of spectral bands, Malpai Site.

Both the SAM and the SMF compare collected spectral data with reference spectra to determine similarity. Because the initial ground truth spectra were collected from a small set of target materials and were not all-inclusive of the materials present in the scenes, the reference library was expanded to include a combination of ground truth spectra and spectra extracted from the Malpai scene. This expanded spectral library was then used for the analysis of additional data sets.

The initial application of the SAM was performed using only the ground truth spectra collected from the T-72 and T-80 tanks, the desert varnish, and a small number of camouflage samples. The results demonstrated that the ground truth spectra provided a good match for some of the materials in the scene. All of the military vehicles were detected as well as many of the tracks left by the vehicles as they were moved into position. However, the algorithm did not correctly identify the vegetation, some of the lighter sand, and portions of the tanks tracks. The vegetation was misclassified as Air Force camouflage and many of the JCCD materials were misclassified due to the lack of appropriate reference spectra. To improve classification accuracy, the reference library was expanded to include extracted spectra from the Malpai data. Spectra representing the desert varnish, the lighter desert sand, vegetation, and a disturbed desert surface resulting from vehicular traffic were extracted from known locations within the Malpai scene. Since the foxhole camouflage and IR appliqué exhibited very distinctive spectral characteristics and did not correspond to any of the ground truth materials, they were also added to the reference library. The use of the expanded reference library improved the results of the SAM analysis dramatically, as expected. Vegetation, variations in desert background, and the JCCD materials were classified with much greater accuracy. False alarms involving misclassification of the desert background and vegetation were also eliminated. Figure 9 (color page) is a portion of the resulting classification image. The tank tracks, portrayed in orange, were clearly distinct from the lighter sand and desert varnish. The vegetation, highlighted in green, was also clearly identified. The improvement in background classification and the reduction in false alarms was achieved at the cost of easily locating all of the threat vehicles. Only four of the T-72s were positively identified as being either T-72 or T-80 targets. The remaining T-72 had only seven of 60 pixels correctly classified as matching the T-72 spectrum.

The SMF was first employed to detect the military vehicles using the ground truth T-72 and T-80 spectra, which differed slightly due to paint scheme and weathering. The slight differences between the T-72 and T-80 spectra were evident in the SMF results. Only three of the five vehicles were positively detected when the T-72 spectra was used, but the vehicles that

were detected were well defined and distinct from the background. All of the target vehicles were detected when the T-80 reference spectrum was used, but the signal-to-clutter ratio was much lower making them harder to distinguish from the background in the resulting filtered image.

Terrain classification was accomplished with the SMF by selecting various background spectra as a reference. However, the use of a single desert varnish reference spectrum allowed several desert features to be characterized simultaneously according to how much they deviated from the reference spectrum. As illustrated by Figure 5, the use of the desert varnish spectrum produced an extensive vehicle traffic assessment. In the figure, the tank tracks appear dark because they differ from the desert varnish which has a deeper restrahlen emissivity minimum.

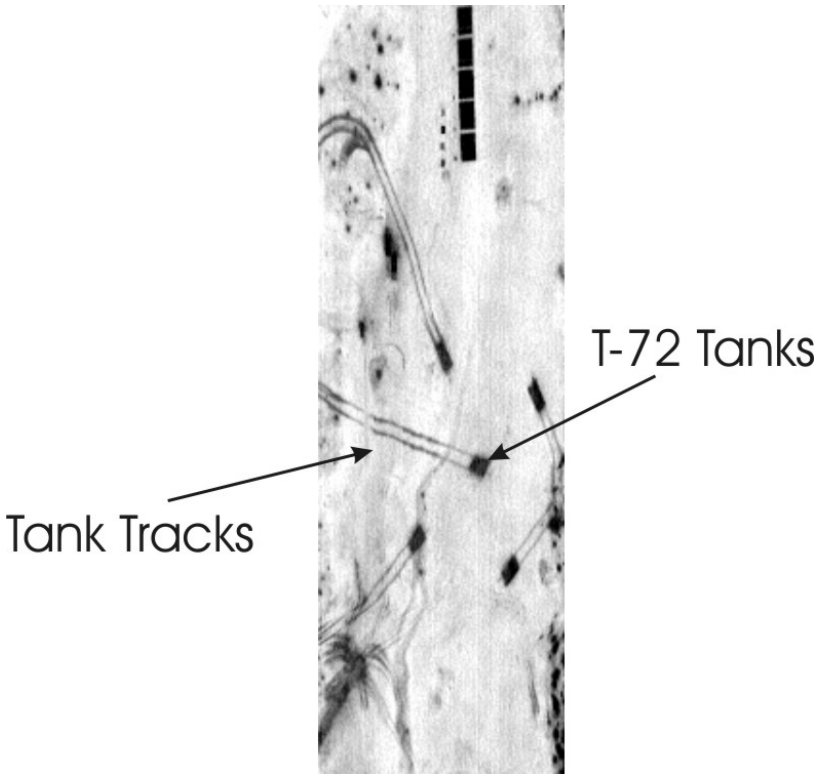

Figure 5. Results of SMF using desert varnish spectrum, Malpai Site.
Bright areas represent matches to reference spectrum.

4.2 Arroyo collection site

The SEBASS collection mission over the Arroyo Collection Site flew directly over the two TBM targets. TBM One was clearly visible in the simulated FLIR image. Its large shape in relation to the surrounding vegetation made it a clear target. A structure just north of the road in the bottom of the image was also identifiable. It corresponded to the location of Tank Four which was covered with a straight-edged thermal space frame. The other target within the field-of-view of the sensor, TBM Two, was not detectable within the FLIR image.

Principal components analysis of the radiometrically calibrated data resulted in the detection of the two TBM targets and Tank Four. The first and second components were similar in behavior to those of the Malpai radiance data sets; highlighting temperature differences and contrasts to desert background, respectively. Both TBM targets were detected in the second and third PCs (Figure 6). The camouflage netting employed over TBM Two was very distinctive resulting in its detection in a large number of subsequent PCs. Although the combination woodland-desert camouflage employed over TBM One was not as spectrally distinct, variations within the netting as well as the boundary between the camouflage and the desert allowed it to be detected in both of these images.

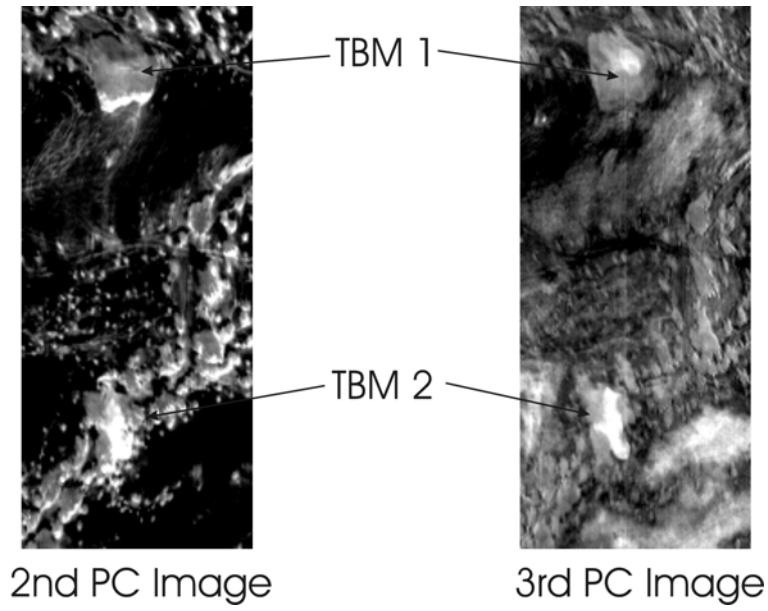

Figure 6. Second and third PCs, Arroyo Site.

The SAM was applied to the emissivity data using the same reference library generated during the SAM analysis of the Malpai data. The resulting classification image is presented in Figure 10 (color page). The algorithm identified the two TBMs and Tank Four. Tank Four and TBM Two were classified as resembling the prototype foxhole camouflage and are portrayed in purple. Examination of the spectra of these targets revealed that their emissive spectra matched that of the foxhole camouflage very closely. TBM One was classified as employing a combination of desert and woodland camouflage. Various tracks and trails were identified. Several woodland camouflage false alarms were noted within some of the vegetation. In addition, an area of disturbed desert sand in the lower right corner of the figure was misclassified as a T-72/T-80 target. Examination of the spectra in this area revealed that it did not match the other desert surface spectra very well. Therefore, the SAM algorithm chose the closest spectra which was the T-72 target spectra.

Application of the SMF also resulted in the characterization of both TBM emplacements and Tank Four. The combination woodland and desert camouflage of TBM One was detected using both the woodland and desert ground truth camouflage spectra. Figure 7 is the resulting filtered image. The darker pixels represent matches to the target spectra. Tank Four and TBM Two were easily detected using the prototype foxhole camouflage.

5. CONCLUSIONS

Analysis of the LWIR spectral data collected by SEBASS during WESTERN RAINBOW resulted in the successful detection of military targets and demonstrated a significant improvement in detection success rate over traditional single-band, infrared FLIR imagery. Both target and background materials were detected, characterized, and classified using standard hyperspectral analysis algorithms historically used for the analysis of data collected within the visible and near-infrared regions of the electromagnetic spectrum.

SEBASS performed extremely well during the exercise. Instrument characterization and calibration efforts allowed spectral analysis to be conducted using ground truth spectra and as well as spectra collected by SEBASS on different days at different times. Although several instrumental artifacts were discovered during the analysis of the WESTERN RAINBOW data, they did not severely degrade the sensor's ability to collect meaningful data. These artifacts were successfully accounted for in software corrections.

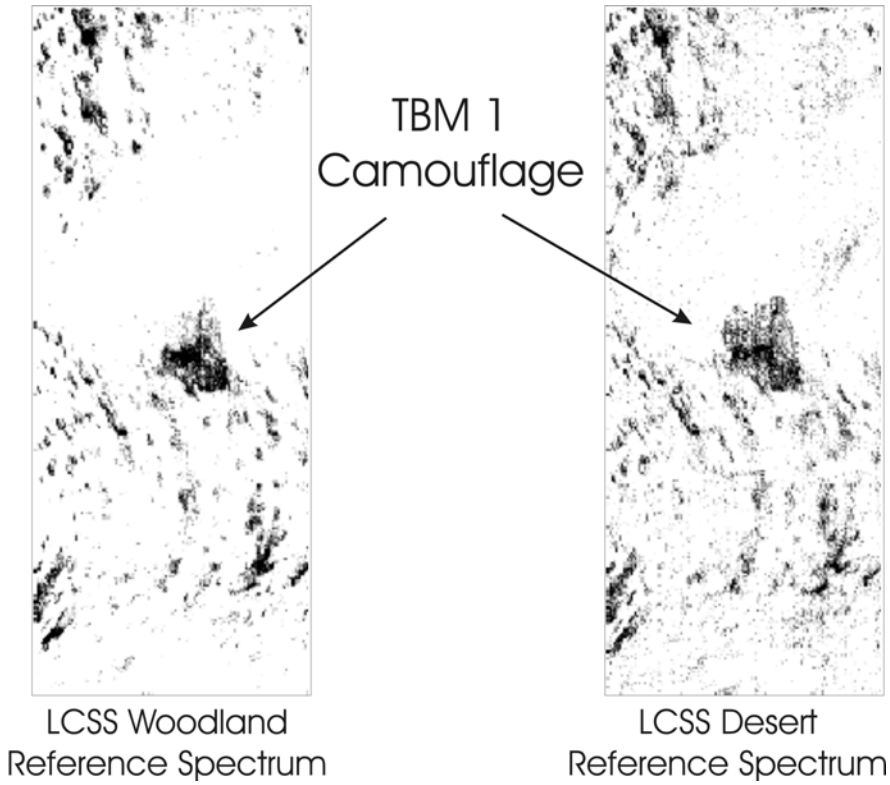

Figure 7. Results of SMF on using LCSS woodland camouflage and LCSS desert camouflage, Arroyo Site. Bright areas represent matches to reference spectrum.

The plastic ruler atmospheric compensation method was designed to operate on data which includes a large amount of near-blackbody materials. The sparse vegetation at the Yuma Proving Ground significantly impacted the algorithm's results. The small number of near-blackbody pixels caused the projection of spectral properties from the majority elements within the scenes, such as sand, onto the derived atmospheric parameters. The parameters then passed these features onto the apparent emissivity spectra during the conversion from radiance measured at the sensor to apparent emissivity.

Principal components analysis demonstrated that SEBASS was capable of collecting thermal spectral data with sufficient spectral and radiometric resolution to detect and discriminate military targets. The analysis revealed that the data collected by SEBASS were not only capable of discriminating between the majority background and man-made materials, but were also capable of discriminating between classes of man-made materials.

The SAM and SMF demonstrated that the conversion to apparent emissivity produced accurate classification results when ground truth spectra and spectra collected from different target sites were used as reference spectra. This was an important result because atmospheric compensation and the derivation of apparent emissivity introduced additional artifacts which may have obscured or altered characteristic spectral features of some of the target materials. The classification algorithms demonstrated the successful detection of various camouflage materials and were successful in categorizing the major terrain features of the desert including vegetation, desert varnish, disturbed sand, and roads and trails. Of the two, the SMF produced the best results. It consistently differentiated between man-made and background materials even in the absence of accurate target spectra. The SAM often mixed the identification of man-made and background materials if insufficient target spectra were employed.

The SAM also had difficulty distinguishing between several of the camouflage materials, the T-72 target spectra, and vegetation. These problems were attributed to the conversion process from atmospherically corrected data to apparent emissivity. The SAM compares spectra by calculating the spectral angle between them. The conversion to apparent emissivity often overestimated surface temperature resulting in slope variations in the derived apparent emissivity spectra. These slope variations resulted in large spectral angle differences and caused the SAM to misclassify spectra which otherwise would have been classified according to small, distinct spectral features.

At a time when battlefield awareness has become a dominant factor in warfare, the capability demonstrated by SEBASS has many applications in military remote sensing. The results of this analysis indicate that an imaging infrared spectral sensor can satisfy key military needs such as target detection and terrain classification.

ACKNOWLEDGMENTS

The authors thank Aerospace Corporation for the opportunity to work with SEBASS in its initial development. Special thanks to Thomas Hayhurst and Bob Johnson also of Aerospace Corporation for sharing their expertise in spectral remote sensing. The authors are also grateful to Wayne Wilson and Sharon Yamasaki of Photon Research Associates for their assistance.

REFERENCES

1. G. Vane, T. G. Chrien, H. T. Enmark, E. G. Hansen, and W. M. Porter, "The Airborne Visible/Infrared Imaging Spectrometer (AVIRIS)", *Remote Sensing of the Environment, Vol* 44, pp. 127-143, 1993.

2. L. J. Rikard, R. Basedow, E. Zalewski, P. Silvergate, and M. Landers, "HYDICE: An Airborne System for Hyperspectral Imaging", *Proc. of Imaging Spectrometry of the Terrestrial Environment,* Vol. 1937, p. 173, 1993.

3. J. Hackwell, D. W. Warren, R. P. Bongiovi, S. J. Hansel, T. L. Hayhurst, D. J. Mabry, M. G. Sivjee, and J. W. Skinner, *LWIR/MWIR Imaging Hyperspectral Sensor for Airborne and Ground-based Remote Sensing,* Aerospace Corporation, El Segundo, CA, 1996.

4. B. H. Collins, *Thermal Spectral Imagery Analysis,* Naval Postgraduate School, Monterey, CA, 1996.

5. Anne B. Kale and Alexander F. H. Goetz, "Mineralogic Information from a New Airborne Thermal Infrared Multispectral Scanner", *Science,* Vol. *222, pp.* 24-27, 1983.

6. R. P. Bongiovi, J. A. Hackwell, T. L. Hayhurst, *Airborne LWIR Hyperspectral Measurements of Military Vehicles,* Aerospace Corporation, El Segundo, CA, 1995.

7. R. P. Bongiovi, *SEBASS Program Brief,* Aerospace Corporation, El Segundo, CA, 1995.

8. B. R. Johnson, *SEBASS Calibration for Western Rainbow Collection,* Aerospace Corporation, El Segundo, CA, 1996.

9. J. Hackwell and T. Hayhurst, *In-scene Atmospheric Compensation of Hyperspectral Data,* Aerospace Corporation, El Segundo, CA, *1995.*

10. M. L. Burke, *Application of Atmospheric Model Corrections to BASS Data,* Aerospace Corporation, El Segundo, CA, 1995.

11. Marcus S. Stefanou, *A Signal Processing Perspective of Hyperspectral Imagery Analysis Techniques,* Naval Postgraduate School, Monterey, CA, 1997.

12. A. Santisteban and L. Munoz, "Applications of Image Principal Component Technique to Geological Study of a Structural Basin in Central Spain", Presented at the Machine Processing of Remotely Sensed Data Symposium, p. 228, 1977.

13. F. A. Kruse, A. B. Lefkoff, J. W. Boardman, K. B. Heidebrecht, A. T. Shapiro, P. J. Barloon, and A. F. H. Goetz, "The Spectral Image Processing System (SIPS) - Interactive Visualization and Analysis of Imaging Spectrometer Data", *Remote Sensing of the Environment,* Vol. 44, pp. 145-163, 1993.

14. Robert A. Schowengerdt, "Multispectral Image Processing", Course from SPIE, Orlando, 1994.

15. Frank P. Billingsley, Anthony Sommese, Kenneth D. Benz, Wayne H. Wilson, and C. Ralph Waters, *MHS Southern Rainbow Data Analysis Report: Task 1,* Photon Research Associates, Inc., pp. 7,8,9-11, 1995.

16. Alan D. Stocker, Irving S. Reed, and Xiaoli Yu, "Multi-dimensional Signal Processing for Electro-optical Target Detection", *Proc of SPIE,* Vol. 1305, pp. 218-231, 1990.

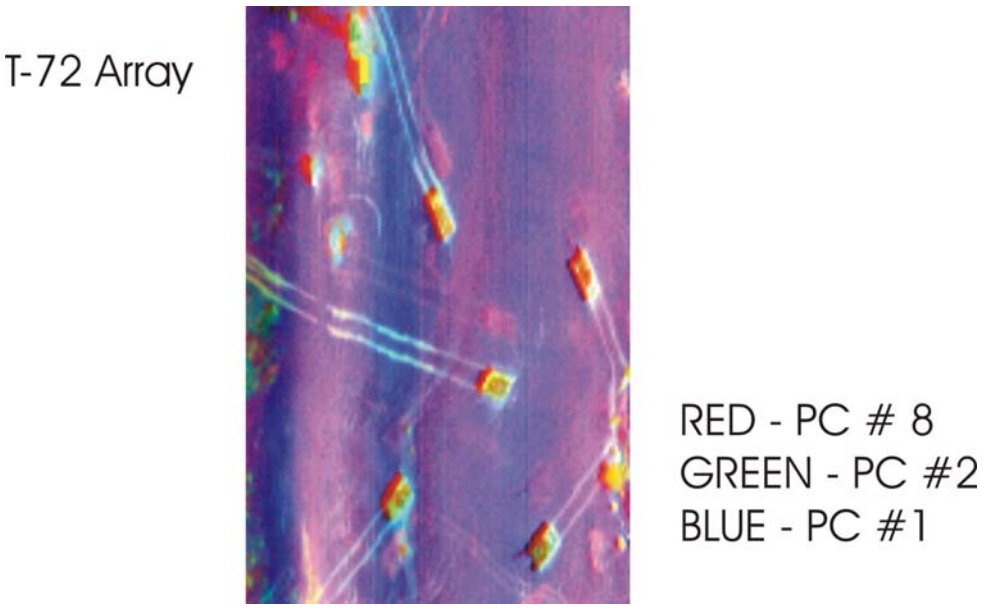

Figure 8. Composite image of PC's one, two, and eight, Malpai Site.

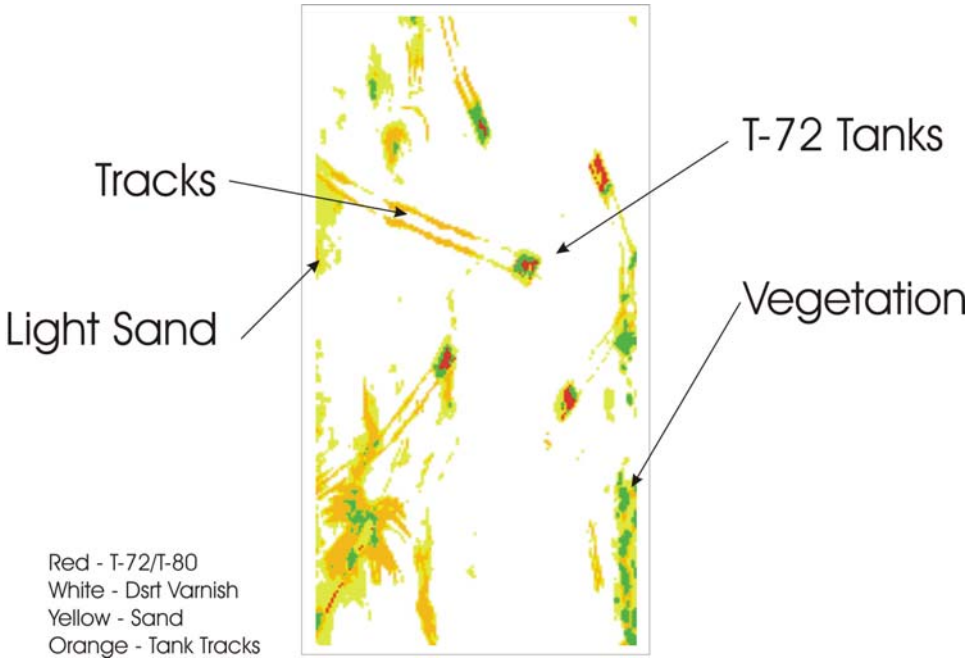

Figure 9. SAM classification image, Malpai Site

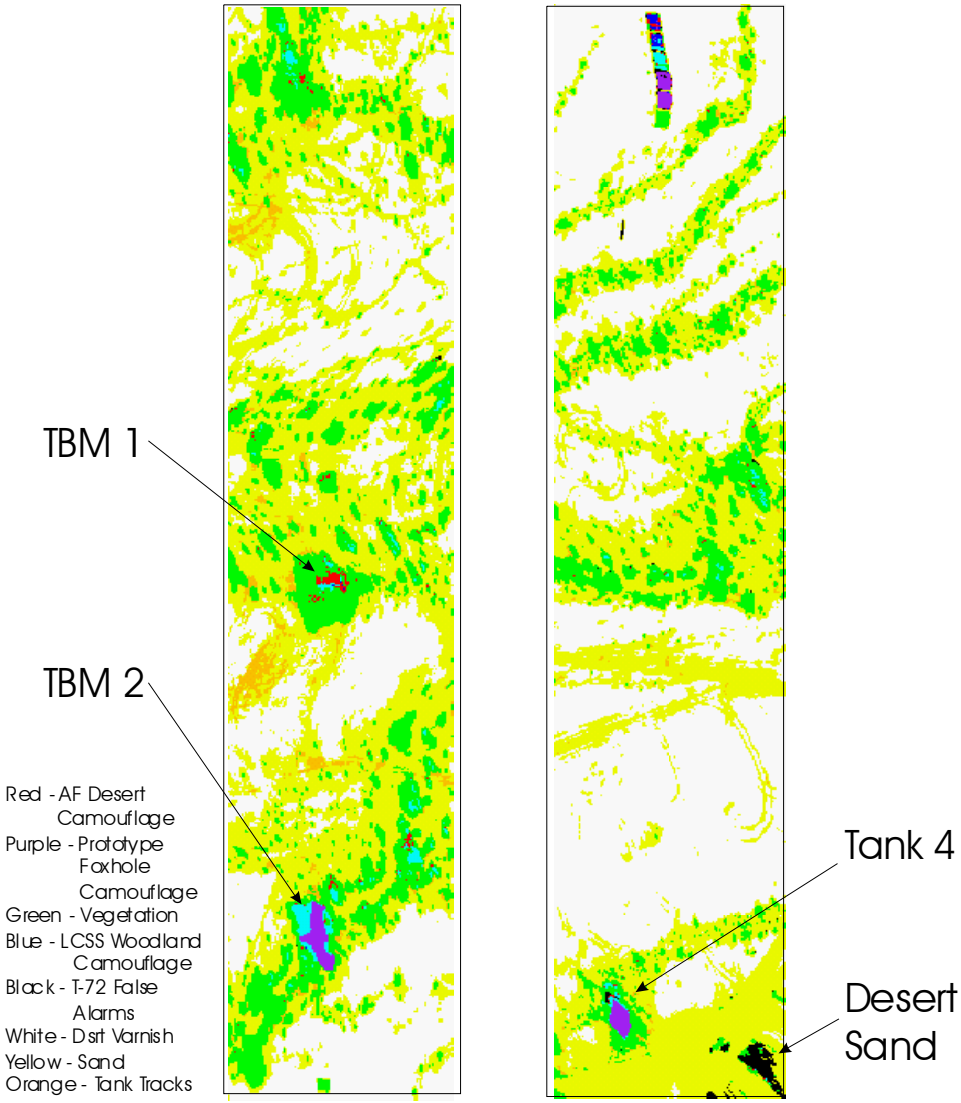

Figure 10. SAM Classification Image, Arroyo Site

SPIE Vol. 3118. 0277-786X/97/$10.00